Influence of Powder Type on Aerosol Emissions in Powder-Binder Jetting with Emphasis on Lunar Regolith for In-Situ Space Applications

Austin C. Hayes,[†] Jorge Osio-Norgaard,[†] Shelly Miller,[†] Marina E. Vance,[*,†,‡] and Gregory L. Whiting[*,†,‡]

†*Paul M. Rady Department of Mechanical Engineering, University of Colorado Boulder*

‡*Corresponding Author*

E-mail: marina.vance@colorado.edu; gregory.whiting@colorado.edu

Abstract

Powder-binder jetting is an additive process with applications for manufacturing complex geometric structures, such as lightweighting, mold making, and in-situ resource utilization (ISRU) for space applications. With this technique, a powder feedstock is spread across a bed during which aerosol may be released leading to human health implications. This study characterizes airborne powder emissions for three powders of varying particle diameters and composition: Hydroperm® gypsum plaster, Lunar Highland Simulant regolith (LHS-1, a lunar soil simulant), and Zeolite 13X (a molecular sieve). Bulk powder D_{50} values were 22 μm for Hydroperm®, 304 μm for LHS-1, and 3.85 μm for Zeolite. Total particle emission rates were $(5.4 \pm 0.96) \times 10^5$ min^{-1} for Hydroperm®, $(1.0 \pm 0.28) \times 10^6$ min^{-1} for Zeolite, and $(2.2 \pm 0.82) \times 10^7$ min^{-1} for LHS-1. An emission factor was developed normalized to the volume of powder

spread resulting in emission factors of 2.8 ± 0.85 $min^{-1}mm^{-3}$ for Hydroperm®, 220 ± 72 $min^{-1}mm^{-3}$ for LHS-1, and 5.0 ± 0.24 $min^{-1}mm^{-3}$ for Zeolite. This indicates that particle emissions from powder-binder jetting machines with a constant spreading mechanism can vary widely depending solely on powder type. In the experimental enclosure where testing took place, LHS-1 PM_{10} concentrations exceeded 8-hour TWA PEL OSHA standards. for crystalline silica by 6-fold indicating that air quality should be a strong design consideration for 3D printing for lunar ISRU. With lower gravitational settling effects, Lunar particulate concentrations 20 m away from the printer were modeled to be 330% higher than on Earth. This study suggests that powder size, morphology, and powder chemistry should be considered holistically when determining emission concerns for new powders in powder-binder jetting. This study also suggests particular attention should be paid to aerosol emissions in a Lunar environment.

Keywords: Powder-Binder Jetting, Particulate Matter, Emission Rate, Additive Manufacturing

Supporting Information Available

Influence of Powder Type on Aerosol Emissions in Powder-Binder Jetting with Emphasis on Lunar Regolith for In-Situ Space Applications

Authors: Austin C. Hayes, Jorge Osio-Norgaard, Shelly Miller, Marina E. Vance, and Gregory L. Whiting

List of Figures

List of Tables

Printer and Enclosure Schematics

An image of the ZCorp 650 used for experimentation is seen in Fig. S1. This printer was selected for its large build volume, low cost as a legacy machine, and high customizablility. The ZCorp 650 includes both the powder-binder jetting components as well as a depowdering station which consists of an airwand and processing chamber for excess powder to be blown off after printing. A schematic of the printer enclosure is seen in Fig. S2. Locations of the OPS, SMPS, and associated tubing connections are shown schematically. Note that air is introduced passively through leaks in the seal to maintain negative pressure as forced ventilation through the HEPA filter is only on the outlet port to maintain particulate-free room air.

Two different objects were printed, a buffalo and a wrench. Both objects were selected as they required similar print times (51 min for the wrench and 1 hr 19 min for the buffalo) and similar layer heights of 100 μm. For this study, as long as a steady state printing profile was achieved, the actual part printed was insignificant. The wrench dimensions were 37 mm x 148 mm x 15 mm (147 layers) and the buffalo dimensions were 74 mm x 48 mm x 21 mm (204 layers). This study allowed us to concurrently test the printability of the zeolite and LHS-1 powders. For the space-relevant powders (z and LHS-1), the wrench was printed in lieu of the buffalo to test the feasibility of in-situ resource utilization with these powders. For the Hydroperm material, the buffalo object was printed.

Figure S1: ZCorp 650 Powder Binder Printer

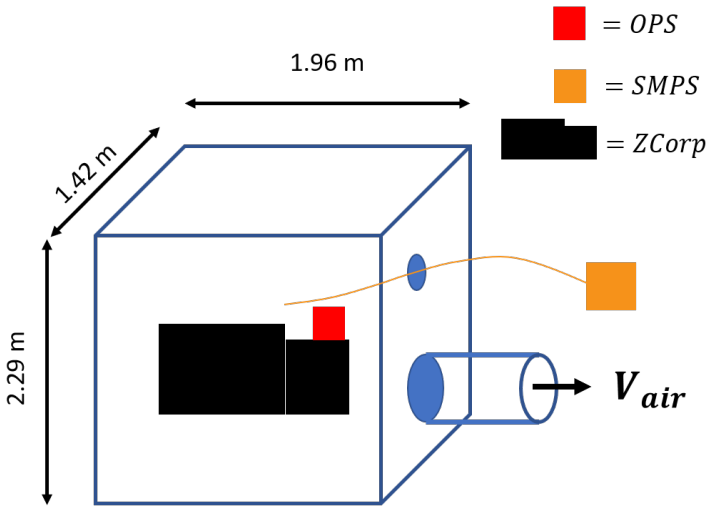

Figure S2: Enclosure and Sensor Schematic

Powder Composition

A breakdown of the three powder types and their composition is shown in Fig. S1

Table S1: Hydroperm®, LHS-1, and Zeolite 13X Powder Composition

	Material/Mineral	Wt %
Hydroperm®	Plaster of Paris ($CaSO_4$ $+1/2$ H_2O)	>70
	Talc	<25
	Portland Cement	<2
	Crystalline Silica	<5
LHS-1	Plagioclase	74.4
	Glass	24.2
	Basalt	0.5
	Limenite	0.4
	Pyroxene	0.3
	Olivine	0.2
Zeolite 13X	$Na_{86}[(AlO_2)_{86}(SiO_2)_{106}] * XH_2O)$	100

EDS Spectra

EDS spectra for Hydroperm®, LHS-1, and Zeolite is shown in Fig. S3-S5. The large carbon and platinum spikes are associated with the carbon-based Epoxy resin used in potting the samples and platinum spin coating to make samples electrically conductive.

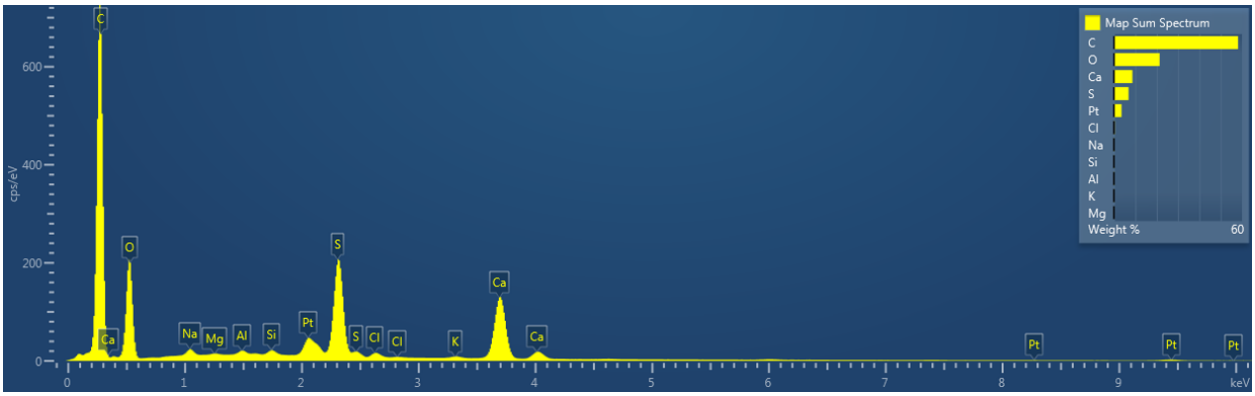

Figure S3: Hydroperm®EDS Spectra

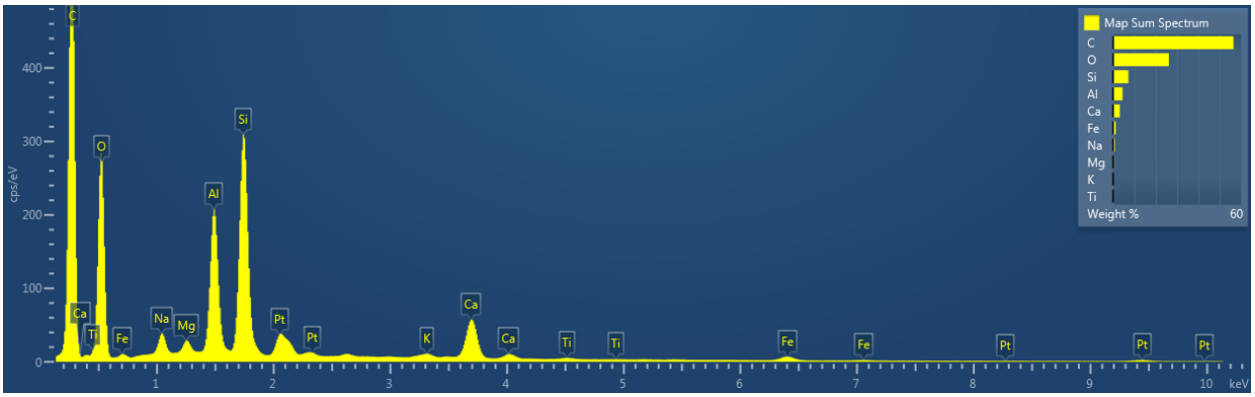

Figure S4: LHS-1 EDS Spectra

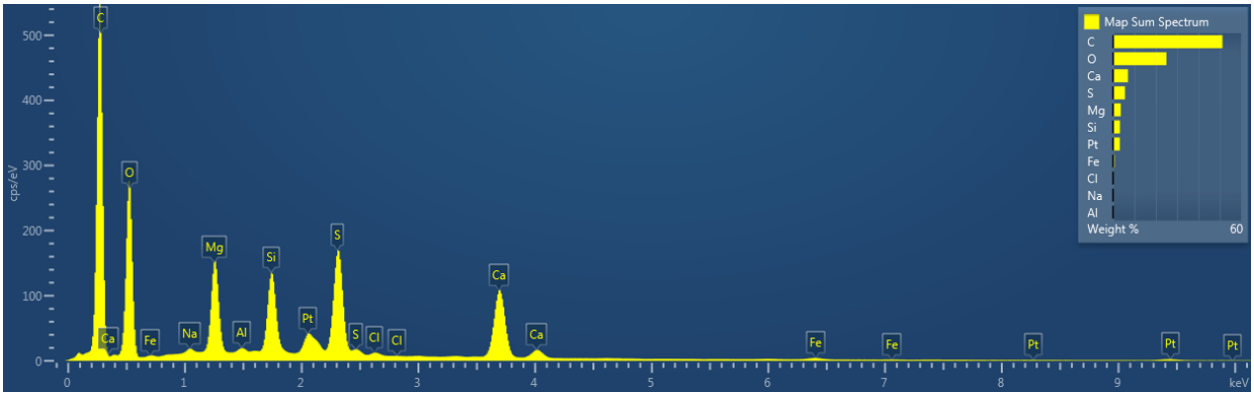

Figure S5: Zeolite EDS Spectra

SMPS Number Concentration

SMPS number concentration heat maps and concentration plots are seen in Fig. S6. For LHS-1 and Zeolite, there are clearly no ultrafine particulate emissions seen visually in the heatmaps and confirmed through low concentrations in the concentration plots. Hydroperm® appeared to have periodic spikes in ultrafine particles; however, this was not associated with printing stage and is also seen during the background period suggesting it is not printer related. Furthermore, number concentrations are at least an order of magnitude lower than other FDM printer studies.[?] As a result, an emission rate cannot be calculated for ultrafine particles as no decay period exists without a source. For this reason, only OPS/APS data was used for analysis of the ZCorp 650 emissions.

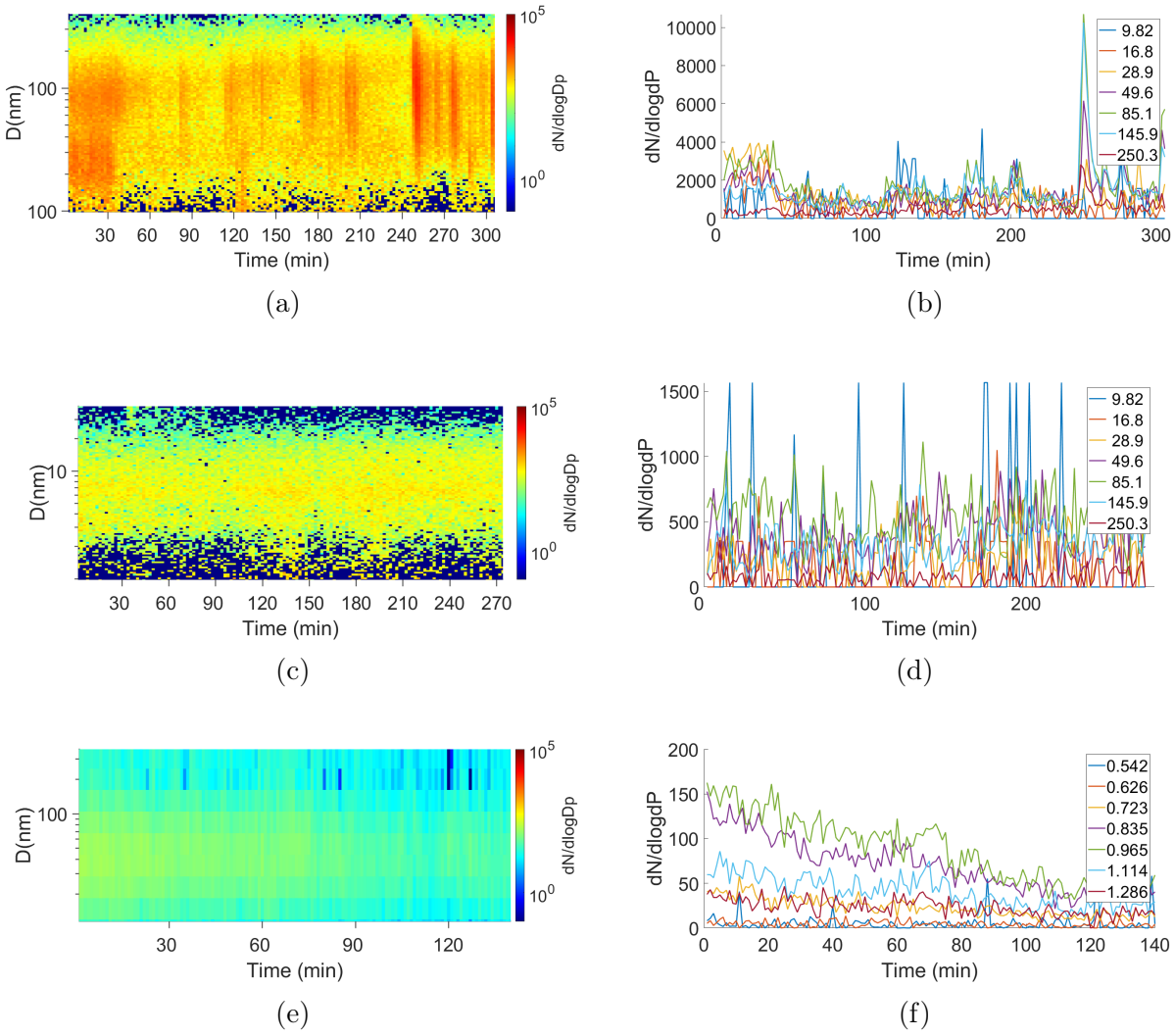

Figure S6: Printing SMPS number concentrations: a). Hydroperm®heat map b). Hydroperm®number concentration plot c). LHS-1 heat map d). LHS-1 number concentration plot e). Zeolite heat map f). Zeolite number concentration plot

Emission Rate Sanity Check Calculations

Due to the atypical flat emission rate curves calculated for each powder type, three different sanity checks were performed to support the findings.

1. *Check #1: Plotting D vs* $\frac{dN}{dlogDp}$

   By plotting the particle diameter versus bin normalized number concentration, we can qualitatively check if concentrations at high bin sizes are similar to lower bin sizes (supporting a flattened emission rate). In Fig. S7, maximum number concentration

is seen to be only 5x higher at 2 μm compared to higher bin sizes.This supports the emission rate being only marginally lower at higher bin sizes.

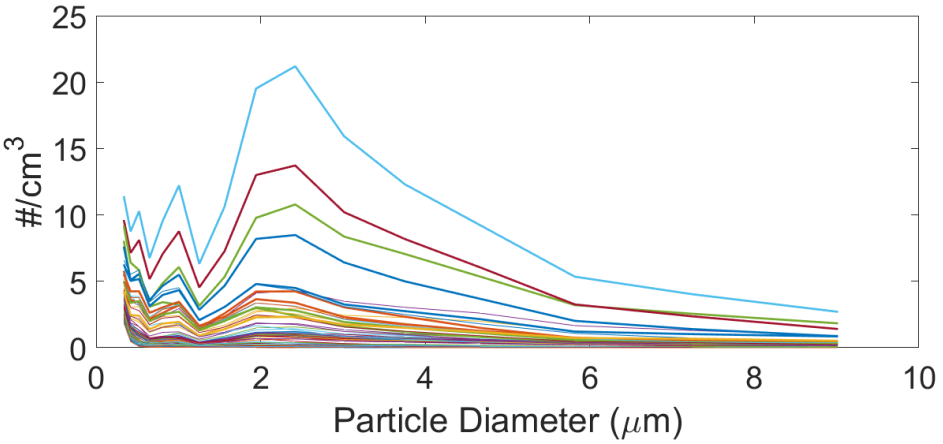

Figure S7: Bin size versus normalized number concentration

2. *Check #2: Measured versus Modeled Number Concentration*

   For a correct emission rate calculation, it should be possible to recreate the printing emissions based off of the experimentally calculated emission rate. To do this, we assumed an average printing concentration throughout the printing regime and found a total emission rate taking the sum of each individual emission rate. For LHS-1, we used a mean loss rate of 0.5 1/min. Fig. S8 depicts the results indicating good agreement between experimental and back calculated data. This is strong evidence to support the validity of the emission rate calculations.

3. *Check #3: Measured versus Modeled Mass Concentration*

   A similar process was conducted for the mass concentration. In this study, emission rate is calculated from number concentration; therefore, mass concentration based off of emission rate will be less accurate. Fig. S9 depicts the measured versus experimental mass concentrations. Results within the same order of magnitude again draws support for the validity of the emission rates.

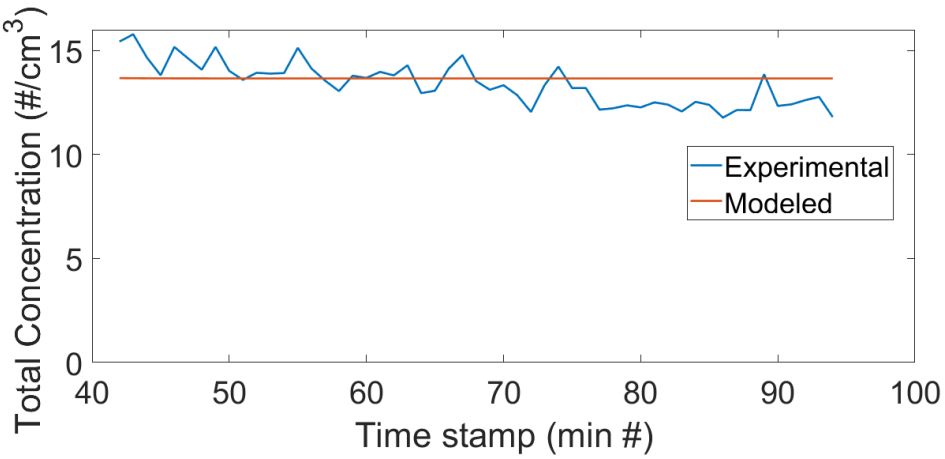

Figure S8: Modeled versus experimental number concentration during printing

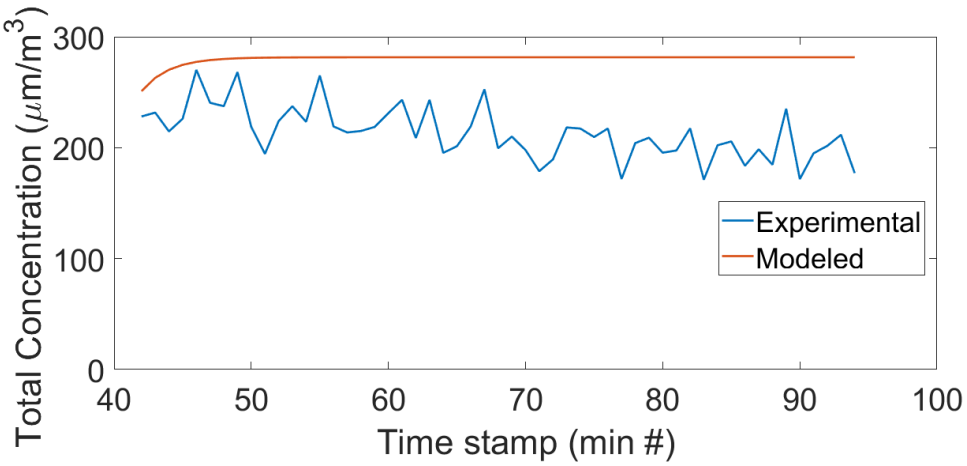

Figure S9: Modeled versus experimental mass concentration during printing

Particle Size Distributions

The PSD for standard ZCorp powder PXL is shown in Fig. S10. Although PXL is not one of the selected powders in this study, it is used by Afshar-Mohajer et al.[?] in a similar air quality of ZCorp printer study. Therefore, understanding how the PSD of PXL compares to this study's PSD of Hydroperm®, Zeolite, and LHS-1 is important to resolve differences in emission rates. Primarily, PXL has a mean powder diameter of 45 μm with a low proportion of fines (<10 μm). This helps to explain why emissions of PXL by Afshar-Mohajer et al.[?] were two orders of magnitude smaller than that of Hydroperm®in this study. A table of D_50 and D_90 values is shown in Fig. S2.

Table S2: Experimental bulk particle sizes and densities of the three tested powders.

Powder	D50 (μm)	D90 (μm)	Density ($g\ cm^{-3}$)
Hydroperm®	21.7 ± 0.54	56 ± 0.54	2.96
LHS-1	304 ± 0.51	820 ± 0.51	1.30
Zeolite	3.85 ± 0.62	9.4 ± 0.62	0.43

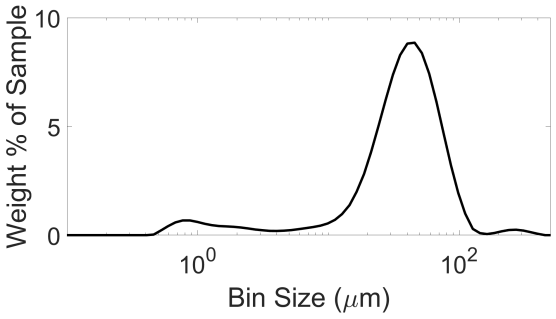

Figure S10: PXL Powder PSD

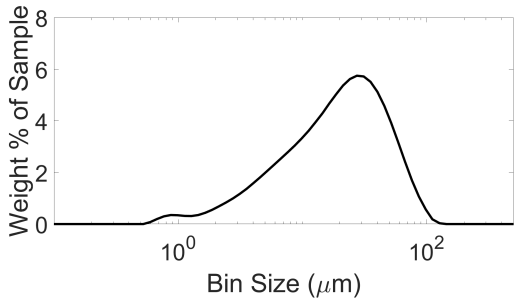

(a)

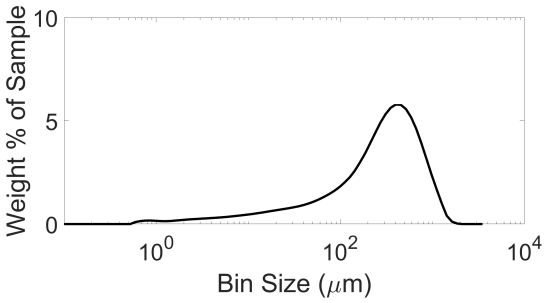

(b)

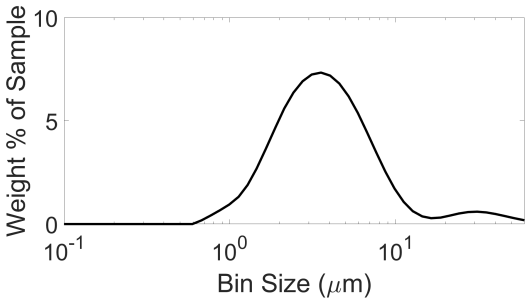

(c)

Figure S11: (a) Hydroperm®PSD (b) LHS-1 PSD (c) Zeolite PSD

Depowdering Mass and Number Concentration

Hydroperm®depowdering mass and number concentration heat map and concentration curves are seen in Fig. S12-S13. Note that larger particles have a larger influence on mass con-

centration; thus, at the same number concentration, larger particles will have a higher mass concentration. During depowdering, PM_{10} rose to $\approx 80\ \mu g\ m^{-3}$ and $PM_{2.5}$ rose to $\approx 11\ \mu g\ m^{-3}$.

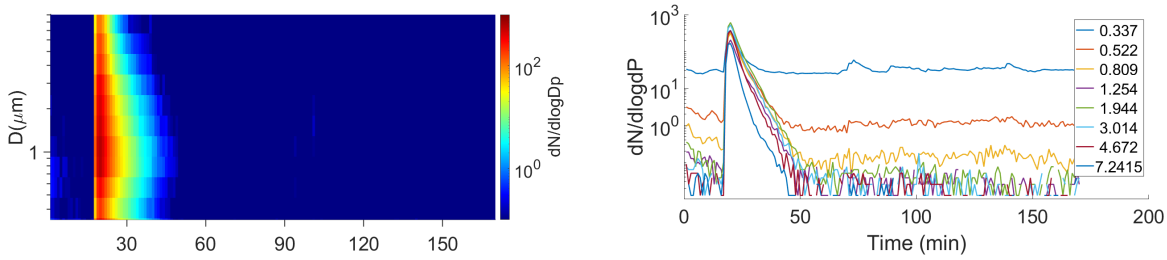

(a) (b)

Figure S12: De-powdering number concentrations for Hydroperm®(a) De-powdering heat map (b) De-powdering number concentration plot

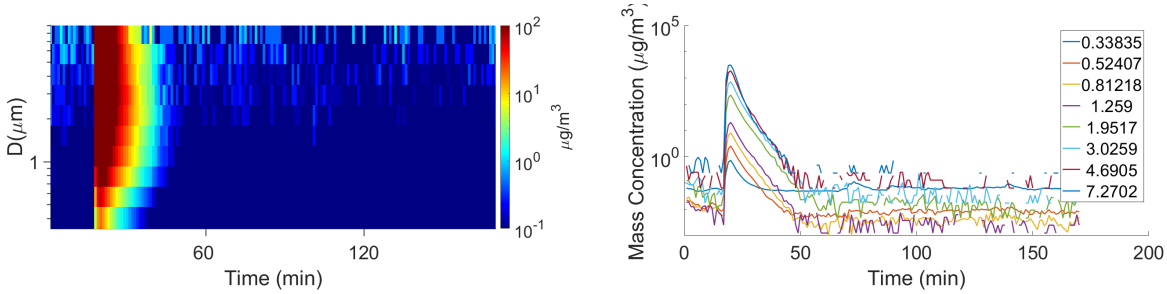

(a) (b)

Figure S13: (a) De-powdering mass heat map for Hydroperm® (b) De-powdering mass concentration curves for Hydroperm

Particulate Matter Mass Concentration by Printing Regime

Powder	Printing Regime	Avg PM2.5 Concentration ($\mu g/m^3$)	Avg PM5 Concentration ($\mu g/m^3$)	Avg PM10 Concentration ($\mu g/m^3$)
Hydroperm	Background	0.514	0.704	1.429
	Filling Bed	1.217 (137%)	5.401 (667%)	18.96 (1227%)
	Printing	0.841 (64%)	2.411 (242%)	6.956 (387%)
	Decay	0.545 (6%)	0.823 (17%)	1.352 (5%)
	All Regimes	0.814 (58%)	2.258 (221%)	6.443 (351%)
LHS-1	Background	0.269	0.488	1.181
	Filling Bed	67.77 (25,093%)	436.5 (89,347%)	1557 (131,737%)
	Printing	14.07 (5,130%)	83.29 (1,697%)	281.6 (23,744%)
	Decay	0.260 (3%)	0.293 (35%)	0.323 (67%)
	All Regimes	4.827 (1,694%)	27.27 (5,488%)	92.62 (8,099%)
Zeolite	Background	0.260	0.318	0.396
	Filling Bed	1.536 (491%)	19.03 (5,884%)	43.10 (10,783%)
	Printing	0.632 (143%)	6.680 (2,000%)	14.14 (3,470%)
	Decay	0.244 (6%)	0.436 (37%)	0.650 (64%)
	All Regimes	0.776 (198%)	6.675 (1,999%)	13.86 (3,400%)

Figure S14: PM concentration by printing regime (% showing increase or decrease from background concentration)

Particulate Simulation Details

Using Flow 3D, a 3m x 3m x 50m rectangular duct was defined with wall boundary conditions. A wall mesh of 0.5 cm was used with increasing mesh size towards the centerline to resolve the boundary layer. Using the hydraulic diameter and the following basic entrance length equations, the laminar entrance length was 316.8 m and the turbulent entrance length was 47.2 m.

$$L_{laminar} = 0.05ReD \tag{1}$$

$$L_{turbulent} = 4.4D(Re^{1/6}) \tag{2}$$

As the Reynolds's number was 2,112, we expect transitioning flow which is seen as a square appearance of the velocity profile across the centerline of the rectangular duct. The simulated transitioning velocity profile is compared to an analytical laminar flow flow profile of the same channel dimensions. A sharper velocity gradient near the walls and leveling off of free stream in the centerline support transitioning flow (Fig. S16). Furthermore, even at fully turbulent flow with an entrance length of 47.2m, we anticipate much if not all of the flow throughout the 50m duct occurs in a developing boundary layer. This will affect particle locations due to a developing velocity profile.

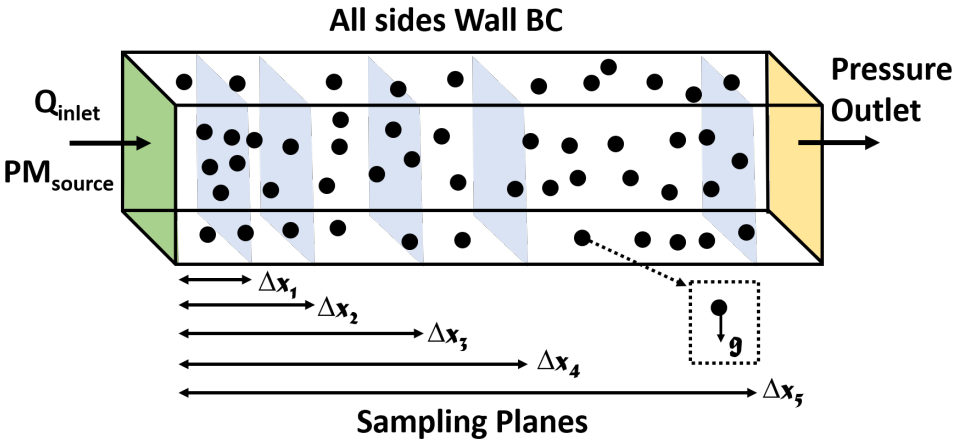

Figure S15: Schematic of CFD Setup

A first-order simulation approach was implemented modeling a plug-flow reactor using commercial code Flow-3D.[?] Inlet boundary condition with 0.7 and 4.4 ACH were employed. To model a printer in the beginning of the reactor, the particulate matter source emits from left to right and particles are carried by the air flow. The initial condition air pressure of the reactor was maintained at 1 atm. Wall boundary conditions were applied at all locations other than the inlet and outlet. Note that the simulation was performed for emissions within a pressurized lunar module, not for the bare lunar environment. A Lagrangian model was used to track 2.2 million particles generated within 5 seconds with emission rates equal to those experimentally calculated. Particle generation was shut off after 5 seconds due to computational limitations. 10 species or bin sizes were simulated (0.522, 0.650, 1.007, 1.562, 2.421, 3.014, 4.672, 5.817, 7.242, and 9.016 μm) PM concentrations were measured at each sampling plane away from the source over time and compared to the reference PM concentration at the generation location. Gravity was reduced to 1.62 m/s^2 and the simulation was performed for 0.7 and 4.4 ACH as well as with 1 and 2 printers in the lunar module. A k-ϵ model was used to measure the turbulence development along the duct. The resulting simulation depicting particle motion colored by velocity can be found in supporting files.

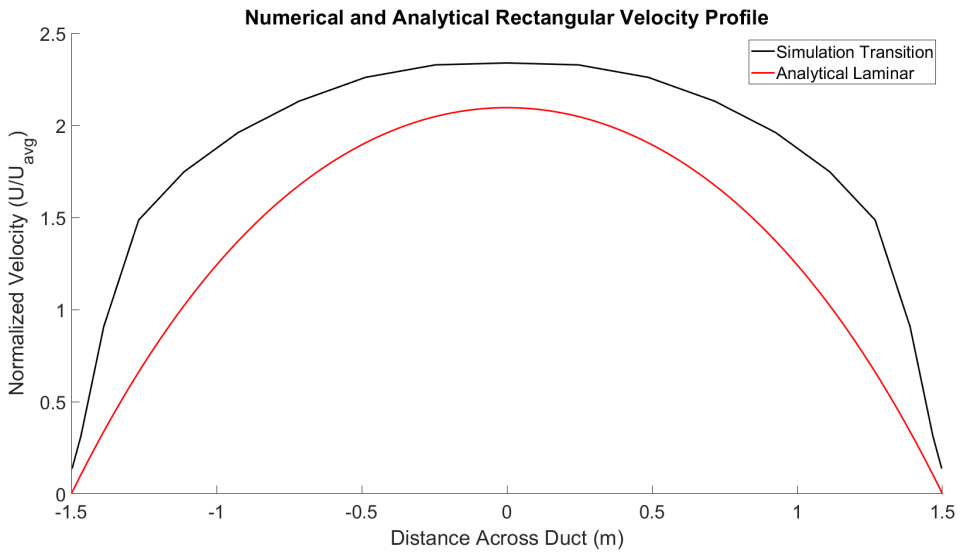

Figure S16: Velocity Profile of Transitioning Simulation and Analytical Laminar Rectangular Duct Flow

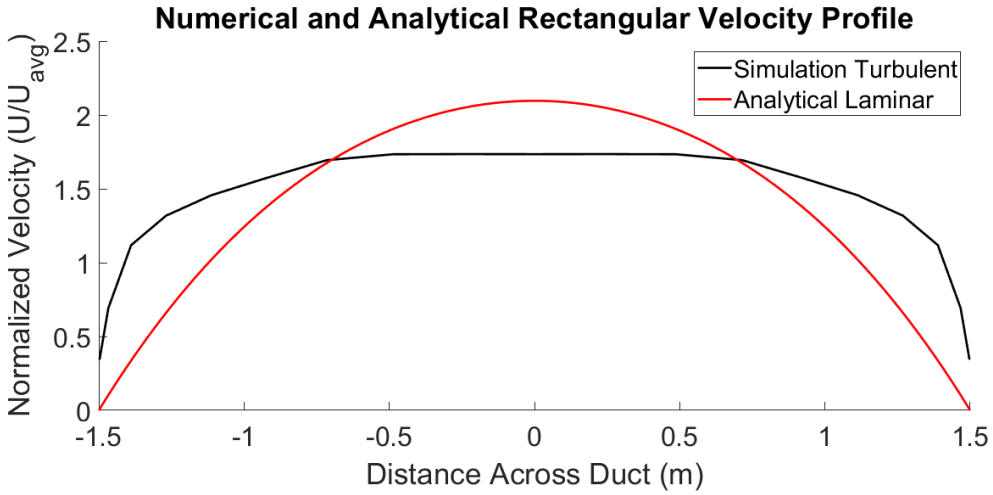

Figure S17: Velocity Profile of Turbulent Simulation and Analytical Laminar Rectangular Duct Flow

Occupational Health Considerations

As powder-binder jetting printers become more common in industrial and office settings, so too does human exposure to them. Furthermore, rarely is only one material desired in manufacturing. Therefore, this study indicates emissions will be variable dependent on the powder type, PSD spectra, chemical makeup, and morphology. In the lack of indoor air

quality standards, we use the national ambient air quality standards set by the USEPA, which imits $PM_{2.5}$ to 35 $\mu g\ m^{-3}$ and PM_{10} to 150 $\mu g\ m^{-3}$ per 24 hrs.[?] We assume the printers are operated continuously in a cycle of a 2 hr job and 40 min set-up between builds. Printing emissions are taken as an average during the printing process and background levels used for the 40 min set-up between builds. Under this scenario, Hydroperm's mean 24 hr $PM_{2.5}$ and PM_{10} (0.81 and 5.3 $\mu g\ m^{-3}$,respectively), would be well below these standards. Zeolite emissions would also lead to low 24-hr average concentrations (0.70 $\mu g\ m^{-3}$ for $PM_{2.5}$ and 16 $\mu g\ m^{-3}$ for PM_{10}). For LHS-1, however, the mean 24-hr concentrations would be 10. and 295 $\mu g\ m^{-3}$ for $PM_{2.5}$ and PM_{10} respectively. In this printing regime, LHS-1 emissions would lead to almost double the ambient standard for PM_{10}. One theory supporting low Hydroperm®and Zeolite emissions is powder with high moisture absorption may lead to enhanced aggregation, limiting the amount of free respirable powder. On the other hand, LHS-1 is a powder that stores little water due to low specific surface area, little nanoporosity, and neither hydrophobic or hydrophilic qualities.[?])

This study suggests that while particle size presence determines particulate matter release, size alone is not an absolute indicator of powder emissions as the powder with the highest powder fraction in the respirable range (Zeolite) did not have the highest emission rate. These results indicate that both powder size and powder properties play a role in emission rate with the highest emitting powder one that is strongly hydrophobic with a P90 particle size in the respirable range ($<$10 μm). It is important to note that these mass concentration values only apply for the ventilation rate of 3.7 ACH and therefore should be used as a reference with mass concentrations for other ventilation scenarios. Additionally, the USEPA limits are for overall PM concentrations and do not account for other PM characteristics, such as composition and morphology. For example, LHS-1 and other regoliths are composed of highly angular particles with a high silica content.

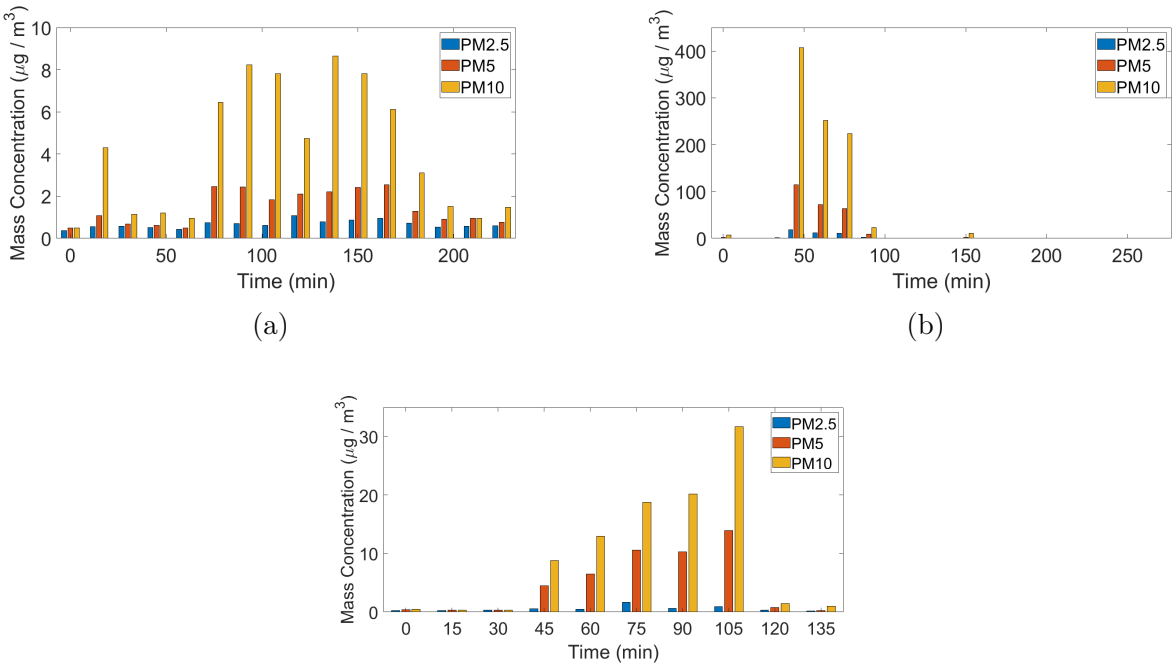

Figure S18: a). Hydroperm®$PM_{2.5}$, PM_5, and PM_{10} over a build cycle b). LHS-1 $PM_{2.5}$, PM_5, and PM_{10} over a build cycle c). Zeolite $PM_{2.5}$, PM_5, and PM_{10} over a build cycle